Emergent Spatial Coordination from Negative Selection Alone:
The Role of Observation Richness in Objective-Free Artificial Life

Anonymous

Abstract

We show that spatial coordination among agents emerges in a multi-agent grid world when agents can observe neighbor states, without any positive behavioral objective guiding the search. Existing artificial life systems typically rely on fitness functions—explicit or implicit—which introduce evaluation bias and constrain the space of discoverable phenomena. We propose an objective-free but viability-filtered approach based on large-scale random rule generation, comparing four observation conditions: random walk, a step-clock control, density-only observation, and state-profile observation. Across 5,000 rules per condition, agents with state-profile observation achieve nonzero median ΔMI (MI calibrated by a permutation-based shuffle null that controls for pair-count bias) while density-only and control agents remain at zero (Cliff's $\delta = 0.355$; median-difference bootstrap 95% CI $[0.078, 0.111]$; Table 3), and the ordering Control $\leq$ Phase 1 $<$ Phase 2 holds across all rule-based comparisons. A Miller-Madow bias-corrected estimator is used throughout, and a shuffle null confirms that the random walk's elevated raw MI is entirely attributable to pair-count bias (ΔMI near zero at 0.050 bits, within the noise floor of the $N = 200$ shuffle null). Moran's I further distinguishes local coordination from large-scale clustering. These results demonstrate that observation channel richness—not rule table capacity or positive-objective selection pressure—drives the emergence of spatial coordination in objective-free but viability-filtered systems.

Submission type: Full Paper

Introduction

Artificial life research aims to understand the principles of living systems by constructing synthetic analogs (Bedau, 2003). A recurring challenge is the role of the objective function: most evolutionary and adaptive systems require an explicit fitness measure that guides search toward "interesting" configurations. Even novelty search (Lehman and Stanley, 2011), which abandons traditional fitness, still uses a novelty metric as an implicit objective.

This reliance on objectives introduces a subtle but pervasive bias. The choice of fitness function constrains which phenomena can emerge, and researchers may inadvertently encode their expectations into the evaluation criteria (Stanley et al., 2019). The question then arises: can meaningful spatial structure emerge in a multi-agent system with no fitness function?

We explore the unexplored quadrant of no positive objective $\times$ viability-only selection, where the only filtering criterion is non-degeneracy—removing rules that produce trivially degenerate simulations (all agents halt or converge to a single state). Crucially, while this negative selection does constitute a minimal selection pressure (surviving rules must avoid complete stasis and global state uniformity), it imposes no behavioral or performance criterion: any surviving rule is equally valid regardless of its spatial structure, MI level, or action distribution. This is analogous to minimal criteria selection (Lehman and Stanley, 2011)—a deliberately weak constraint that shapes the set of viable rules without specifying what is desirable.

Our core contribution is threefold:

1. A minimal grid-world model with objective-free negative selection, where random rule tables are evaluated and only degenerate ones (halt or state-uniformity) are discarded.

2. Evidence that observation richness—the amount of neighbor state information available to agents— drives emergent spatial coordination, independent of

rule table capacity.

3. Robustness across four experimental conditions and 20,000 rule evaluations, with statistical significance confirmed by Mann-Whitney U tests with Holm-Bonferroni correction.

Related Work

Self-organization without selection. Cellular automata such as Conway's Game of Life (Gardner, 1970) and Wolfram's elementary rules (Wolfram, 1984) demonstrate that simple local rules can produce complex global patterns. Continuous extensions like Lenia (Chan, 2019) show rich morphogenetic dynamics in continuous state spaces. Reynolds' Boids (Reynolds, 1987) produce flocking behavior from three local rules. These systems share a common trait: the rules are hand-designed, not discovered through search.

Evolutionary ALife with fitness. Tierra (Ray, 1991) and Avida (Ofria and Wilke, 2004) use implicit fitness through resource competition and self-replication. While these systems produce open-ended dynamics, the replication criterion itself acts as a fitness function that selects for self-replicating programs.

Novelty search and open-endedness. Novelty search (Lehman and Stanley, 2011, 2008) replaces fitness with a novelty metric, enabling discovery of diverse behaviors. The open-ended evolution community has explored various approaches to sustaining innovation (Taylor et al., 2016; Stanley et al., 2019). However, all such approaches still employ an evaluation function—whether fitness, novelty, or complexity. The minimal criteria framework (Lehman and Stanley, 2011) uses deliberately weak constraints to avoid trivial solutions without imposing performance objectives—our viability filtering is directly analogous.

Information-theoretic measures. Mutual information and transfer entropy have been used to quantify coordination in multi-agent systems (Lizier et al., 2012). We use mutual information as a post-hoc analysis tool, never as a selection criterion.

Our position. Our approach differs from all the above by using no positive objective —not fitness, novelty, or complexity as an optimization target. We generate random rules, discard only degenerate ones (halt or state-uniformity), and ask what structure the surviving rules exhibit.

Methods

World Model

The simulation environment is a 20×20 toroidal grid populated by 30 agents (Figure 1). Each agent occupies exactly one cell (no overlap allowed) and maintains an internal state $s \in \{0, 1, 2, 3\}$. At each of 200 time steps, agents are updated in a random sequential order: one agent at a time observes its local neighborhood, looks up an action in a shared rule table, and executes it. The action space comprises 9 mutually exclusive actions: 4 cardinal movements, 4 state changes, and a no-op. Movement to an occupied cell fails silently.

Table 1: Model and experiment parameters.

Parameter	Value
Grid topology	20×20 torus (von Neumann)
Number of agents	30 (7.5% density)
Internal states	$\{0, 1, 2, 3\}$
Action space	9 (4 moves, 4 state changes, 1 no-op)
Simulation steps	200
Update order	Random permutation each step
Halt window	10 consecutive unchanged steps
MI estimator	Miller-Madow corrected, base-2 (bits)
Shuffle null N	200 permutations per rule
Seeds per condition	5,000 (rule seed i, sim seed i)

Observation Phases

We compare four observation conditions that vary in the information available to agents:

Random Walk (RW). Each agent selects an action uniformly at random from $\{0, \ldots, 8\}$ at every step, ignoring the rule table entirely. (Reported as "5,000 seeded runs" rather than rules, since no rule table is consulted.) This baseline isolates the contribution of grid geometry (collision avoidance, toroidal wrapping) from rule-driven behavior, and also serves to calibrate the MI estimator under conditions with minimal spatial clustering.

Control (step-clock). Agents observe their own state $s \in \{0, \ldots, 3\}$, the count of occupied von Neumann neighbors $n \in \{0, \ldots, 4\}$, and a periodic step clock $t \bmod 5 \in \{0, \ldots, 4\}$. The rule table has $4 \times 5 \times 5 = 100$ entries. The step clock is non-informative about neighbor identity or state—a global clock can induce temporal synchrony but carries no spatial information about
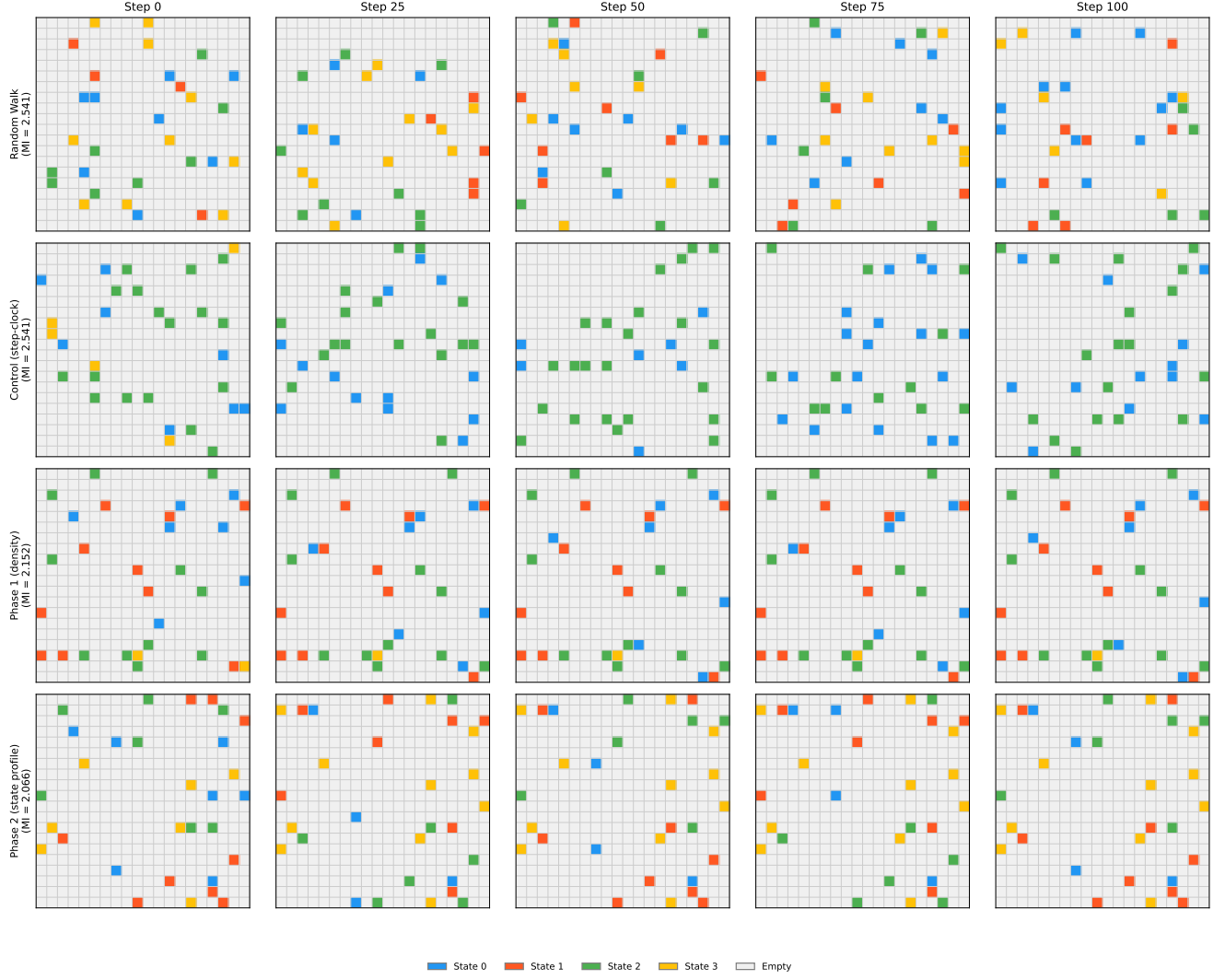
Figure 1: Grid snapshots of hand-picked highest-ΔMI surviving rules from each condition (final-step grid; Miller-Madow estimator). Raw MI values shown are for individual top-performing rules, not condition medians; see Table 2 for population statistics. RW and Control panels may show similar elevated raw MI—this is expected, as raw MI is inflated by pair-count bias; ΔMI (Table 2) correctly shows near-zero calibrated values for both. Each panel shows the 20×20 toroidal grid with agents colored by internal state. Phase 2 rules produce visibly clustered spatial patterns, while Control rules appear disordered.

neighbors. It serves as a capacity-matched third dimension that reaches Phase 2's table size without adding any spatial content.

Phase 1: density-only (P1). Agents observe their own state s and neighbor count n. The rule table has $4 \times 5 = 20$ entries, indexed by $5s + n$. This is the minimal observation that couples agents spatially.

Phase 2: state profile (P2). Agents observe their own state s, neighbor count n, and the dominant neighbor state $d \in \{0, \ldots, 4\}$ (the most frequent state among occupied neighbors, with ties broken by smallest value; 4 denotes no occupied neighbors). The rule table has $4 \times 5 \times 5 = 100$ entries, indexed by $25s + 5n + d$.

Viability Filters

Only two filters are applied, both enforcing non-degeneracy rather than behavioral quality:

1. Halt detection: If all agents' positions and states remain unchanged for $W = 10$ consecutive steps, the simulation is terminated. Applied uniformly from step 1 with no burn-in.

2. State uniformity: If all 30 agents share the same internal state at any step, the simulation is terminated. Global homogeneity is the criterion; partial uniformity is not penalized.

These filters are applied identically across all four conditions and all density levels. Any surviving rule may exhibit any spatial pattern, MI value, or action distribution; the filters exclude only dynamical trivialism (complete stasis or indistinguishable agents). No fitness function, novelty metric, complexity threshold, or behavioral criterion is used at any stage. Across 5,000 rules per condition, survival rates are: Random Walk 100%, Phase 1 71.4%, Phase 2 74.7%, Control 44.5%. Operationally, these filters enforce viability constraints only: they remove degenerate trajectories but do not reward any specific spatial pattern, information score, or task completion behavior. All coordination metrics are computed after filtering and are never fed back into search.

Metrics

All metrics are computed post-hoc and never used for selection:

Neighbor mutual information (MI). For each pair of adjacent occupied cells (i, j) on the toroidal grid, we compute the mutual information between their internal states:

$$I(S_i; S_j) = \sum_{s_i, s_j} p(s_i, s_j) \log_2 \frac{p(s_i, s_j)}{p(s_i) \, p(s_j)} \qquad (1)$$

where the joint and marginal distributions are estimated from all adjacent occupied pairs at a given time step. To mitigate the positive bias of the plug-in estimator at small sample sizes, we apply the Miller-Madow correction (Miller, 1955): $\hat{I}_{\mathrm{MM}} = \hat{I} - (K_{\mathrm{joint}} - K_X - K_Y + 1)/(2n \ln 2)$, where K_{joint}, K_X, and K_Y are the counts of non-zero bins in the joint and each marginal distribution respectively, and n is the number of pairs. Values are clamped to ≥ 0. Concretely: the random variables are the internal states of both agents in each occupied adjacent pair at the final simulation step (step 200). All occupied neighbor pairs at that step are pooled and MI is computed once from the aggregate joint count—not averaged over per-step estimates. MI is not conditioned on density; pair-count bias is controlled via the shuffle null instead. High MI indicates that neighboring agents' states are statistically dependent—a signature of spatial coordination.

Interpreting ΔMI as coordination. Neighbor ΔMI measures local statistical dependence between adjacent agents' states beyond chance. A positive ΔMI indicates state assignments are not spatially random. Crucially, ΔMI alone does not distinguish dynamic coordination from frozen clustering: a world where agents freeze in correlated positions would also yield high MI. We address this via two complementary analyses: (i) temporal MI trajectories (Figure 3) distinguish frozen early-plateau dynamics (Phase 1) from sustained dynamic coordination (Phase 2), and (ii) transfer entropy (supplementary material) confirms directional information flow in Phase 2 beyond symmetric MI. The viability filter further rules out the most trivial high-MI scenario by explicitly removing state-uniform worlds.

Shuffle-null MI calibration. To control for pair-count bias—where configurations with few neighbor pairs produce inflated MI estimates regardless of state structure—we compute a permutation-based shuffle null. For each rule's final snapshot, we fix occupied positions and randomly reassign states among them $N = 200$ times, computing $\hat{I}_{\mathrm{MM}}$ for each shuffle. Specifically, the shuffle operator preserves: (i) the set of occupied positions, (ii) the neighbor-pair graph structure, and (iii) the marginal state-frequency counts; it permutes only the assignment of states to positions. The mean across shuffles is the shuffle-null MI. The calibrated ΔMI is then:

$$\Delta\mathrm{MI} = \hat{I}_{\mathrm{MM}} - \bar{I}_{\mathrm{shuffle}} \qquad (2)$$

which isolates genuine spatial coordination from estimation artifacts. Unlike a rectified (max(0)) version, the unrectified ΔMI allows negative values when the observed MI falls below the shuffle null, providing an unbiased view of the full distribution. Specifically: positions are fixed; states among occupied cells are uniformly permuted; $\hat{I}_{MM}$ is computed for each of $N = 200$ shuffles; $\overline{I}_{\text{shuffle}}$ is the mean over those shuffles. The Miller-Madow correction is applied independently to both the observed MI and each shuffle replicate before averaging. All MI values are in bits (base-2 logarithm). In particular, the random walk's high raw MI (≈ 0.91 bits) is entirely attributable to pair-count bias: ΔMI near zero (0.050 bits, within the noise floor of the $N = 200$ shuffle null).

Same-state adjacency fraction. Because agent states are categorical (nominal), traditional Moran's I is inappropriate—it treats states as numeric, computing deviations from an arithmetic mean. We therefore report the same-state adjacency fraction (a join count statistic): the fraction of occupied neighbor pairs sharing the same internal state, bounded in $[0, 1]$. This is the standard spatial autocorrelation measure for categorical data.

Moran's I. Spatial autocorrelation is quantified by Moran's I (Moran, 1950) across occupied cells using torus 4-neighborhood weights: both cells must be occupied for a weight of 1. Values range from -1 (dispersed) through 0 (random) to $+1$ (clustered). As noted above, Moran's I treats states as numeric and is therefore a secondary indicator; the same-state adjacency fraction is the primary categorical spatial statistic.

State entropy. Shannon entropy (Cover and Thomas, 1991) of the internal state distribution across all agents: $H = -\sum_s p(s) \log_2 p(s)$.

Action entropy. Per-agent Shannon entropy of the cumulative action distribution, summarized as the mean and variance across agents.

Experimental Design
For each of the four conditions, we generate 5,000 random rule tables using deterministic seeds (rule seeds 0–4,999, simulation seeds 0–4,999). Each rule table is evaluated on a single 200-step simulation. Surviving rules (those not terminated by halt or state-uniformity filters) have their final-step metrics recorded; all pairwise statistical comparisons use only surviving rules.

Statistical comparisons use two-sided Mann-Whitney U tests (Mann and Whitney, 1947) with Holm-Bonferroni correction (Holm, 1979) applied across all metrics within each pairwise comparison. Each pairwise comparison (e.g., P1 vs. P2) tests a distinct hypothesis about the effect of observation content, so correction is applied per comparison rather than globally across all stages. Effect sizes are reported as Cliff's δ (Cliff, 1993) (equivalent to rank-biserial correlation for Mann-Whitney U): $\delta = 1 - 2U_A/(n_1 n_2)$, where U_A is the U statistic for the first-listed group. To replace extreme p-values with more informative measures, we report bootstrap 95% confidence intervals (Efron, 1979) for the median difference (10,000 resamples, percentile method) as the primary effect-size statistic; p-values are retained as secondary evidence. Each rule table is paired with a single simulation seed (rule seed i paired with simulation seed i), so per-rule conclusions reflect one initial configuration.

Results
Evidence Ladder Among Rule-Based Conditions
Table 2 and Figure 2 present the neighbor mutual information across all four conditions. Among the three rule-based conditions, Phase 2 separates clearly from both baselines. A smaller but statistically detectable shift also holds between Phase 1 and Control (Cliff's $\delta = 0.124$; see Table 3), though both share median ΔMI $= 0$ and the practical coordination difference is negligible. The ordering is:

$$\text{Control} < \text{Phase 1} < \text{Phase 2}$$

The control condition, despite having 100-entry tables (equal to Phase 2), produces zero median ΔMI—demonstrating that table size alone is insufficient. Phase 2 is the only rule-based condition with nonzero median ΔMI, driven by access to neighbor state information (Table 3; bootstrap 95% CI excludes zero).

Random Walk Baseline and Shuffle-Null Calibration
All MI values in this paper use the Miller-Madow bias-corrected estimator (Miller, 1955), which subtracts a first-order correction term from the naive plug-in estimate. However, this correction becomes insufficient when the number of neighbor pairs n is comparable to the number of joint-distribution bins K—precisely the regime of random-walk agents, where $\approx$4–5 adjacent pairs populate up to 16 joint categories.

The expected pair count varies substantially by condition: at the final step (step 200), the mean $\pm$ SD number of occupied adjacent pairs is 4.3 ± 1.9 for Random Walk, 3.9 ± 3.6 for Control, 11.0 ± 8.1 for Phase 1, and 12.0 ± 7.3 for Phase 2. Phase 1 and Phase 2 produce far more adjacent pairs than the baselines because rule-driven agents tend to aggregate; yet their ΔMI values differ dramatically (0.000 vs. 0.096 bits), confirming

Table 2: Calibrated neighbor mutual information and spatial clustering by condition. $\Delta\text{MI} = \text{MI}_{\text{observed}} - \text{MI}_{\text{shuffle null}}$ is the primary calibrated metric controlling for pair-count bias (5,000 rules per condition, $N = 200$ shuffles). Raw MI values use the Miller-Madow bias-corrected estimator and are reported secondarily. The random walk's high raw MI is entirely attributable to pair-count bias ($\Delta\text{MI} \approx 0.050$ bits, within the shuffle-null noise floor).

Condition	Table Size	Median ΔMI	Median MI	Median Adj. Frac.[1]	Frac. ΔMI > 0	Survival
Random Walk	1 (unused)	0.050	0.910	0.364	52%	100.0%
Control	100	0.000	0.000	0.329	14%	44.5%
Phase 1	20	0.000	0.019	0.291	29%	71.4%
Phase 2	100	0.096	0.298	0.350	58%	74.7%

that the difference reflects state structure rather than sample-size effects.

The shuffle null resolves this directly. By permuting states among fixed positions ($N = 200$ shuffles per rule), we obtain the expected MI under the null hypothesis of no spatial state structure. The calibrated $\Delta\text{MI} = \text{MI}_{\text{observed}} - \overline{\text{MI}}_{\text{shuffle}}$ isolates genuine coordination from pair-count artifacts (see Eq. 2).

For the random walk, ΔMI is near zero (0.050 bits) (Table 2), confirming that its elevated raw MI is entirely attributable to pair-count bias—not spatial structure. In contrast, Phase 2 retains substantial ΔMI, demonstrating genuine coordination that persists after bias calibration. Notably, the Control condition—not Phase 2—has the highest median Moran's I (0.124), reflecting clustered but uncoordinated spatial patterns from its large table size. Phase 2's median Moran's I (-0.020) is near zero, indicating that its elevated MI arises from local state coordination among neighbors rather than from large-scale spatial clustering.

The random-walk baseline remains informative: it validates the shuffle-null calibration procedure, establishes the bias floor, and confirms that all 5,000 random-walk rules survive (100% survival rate) since random actions never trigger halt or state-uniformity filters.

Table-Size Confound Resolved

A natural objection is that Phase 2's higher MI could result from its larger rule table (100 entries vs. 20 for Phase 1), which permits more complex behaviors. The control condition resolves this confound directly: it uses 100-entry tables—identical in size to Phase 2—but replaces the informative dominant-neighbor-state dimension with a non-informative step clock. The control produces lower MI than Phase 1 despite having 5× more table entries. This demonstrates that observation content, not table capacity, drives emergent coordination.

The pairwise comparisons confirm this (Table 3): Phase 1 produces significantly higher MI than Control despite having smaller tables, and Phase 2 vastly exceeds Control despite equal table size.
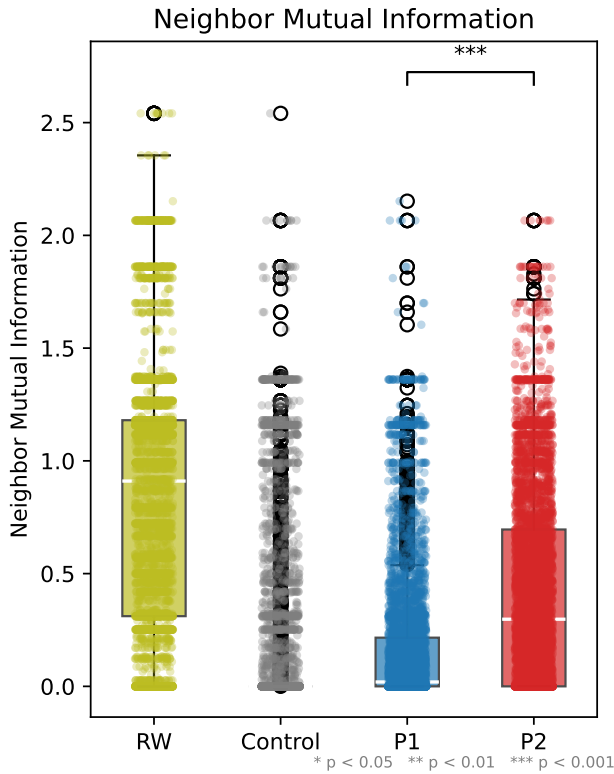

Figure 2: Final-step neighbor MI (Miller-Madow corrected, bits) distributions across rule-based conditions. Box plots with scatter strips show the full distribution for surviving rules. The evidence ladder Control < P1 < P2 is clearly visible.

Filter-Selection Confound Check

A key methodological concern is that viability filters might indirectly favor high-MI rules, creating an apparent Phase 2 advantage through selection bias. To test this directly, we measured point-biserial correlation between survival status and final-step MI within each condition. The correlations are nearly identical for Phase 1 and Phase 2 ($r \approx 0.14$ in both), while Control is higher ($r = 0.45$) due to its substantially lower survival rate. The relevant comparison is therefore Phase 1 vs. Phase 2: because their filter–MI coupling is matched, the Phase 2 excess-MI advantage cannot be explained by differential filter selection.

Ranking-Stability Overlap Interpretation

Post-merge follow-up analysis reports Kendall-τ stability with explicit overlap diagnostics across seed batches. For Phase 2 in the archived follow-up run, compared seed batches show zero shared surviving rule IDs under the selected alignment key, so τ is undefined and reported as N/A. This indicates non-identifiability (insufficient overlap), not negative rank correlation.

Temporal Dynamics

The four conditions exhibit qualitatively distinct temporal behaviors (Figure 3):

- Phase 1: MI rises quickly then plateaus—"frozen" dynamics where spatial patterns crystallize early.

- Phase 2: MI rises and remains dynamic, with ongoing fluctuations—sustained spatial coordination without freezing.

- Control: Highly chaotic trajectories with large MI variance and frequent collapses to zero.

- Random Walk: High but flat MI throughout, reflecting constant estimation bias from few adjacent pairs rather than genuine coordination.

This pattern is an exploratory qualitative observation only. It is consistent with a possible frozen–dynamic–chaotic ordering across conditions, but we do not claim edge-of-chaos evidence here because the analysis is based on a small sample of top-performing rules and does not include quantitative criticality measures (e.g., Lyapunov exponents).

Seed Robustness

To confirm that condition-level differences reflect rule properties rather than single-seed outcomes, we re-evaluated the top 50 rules from each rule-based condition across 20 independent initial seeds (1,000 simulations per condition). Among Phase 2 rules, 84% maintain positive median ΔMI across seeds (mean $P(\Delta$MI $>$
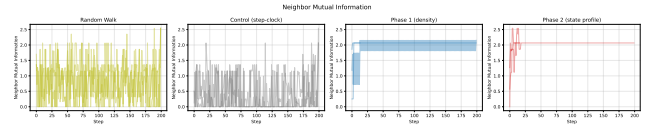

Figure 3: MI time-series trajectories for top-3 rules per condition. Phase 1 freezes early, Phase 2 remains dynamic, and Control shows chaotic fluctuations.

$0) = 0.748$). For Phase 1 and Control, the corresponding figures are 36% and 44% respectively. The Phase 2 ΔMI advantage is not seed-specific: the condition ordering is preserved regardless of initial configuration.

Coordination Archetypes

To characterize what kind of coordination Phase 2 produces, we examined top-performing rules and temporal trajectories, identifying three recurring coordination patterns:

1. State-propagation dynamics. Agents propagate the dominant neighbor state across the grid, producing traveling wavefronts of state transitions. These rules show high ΔMI, moderate same-state adjacency fraction, and sustained MI fluctuations (consistent with Phase 2's dynamic temporal trajectory).

2. Frozen coordination (majority-locking). Agents rapidly converge to a dominant state and freeze, yielding high but static MI. This pattern resembles Phase 1 behavior but arises via state-dependent rather than density-only rules.

3. Persistent boundary structures. Stable clusters form at domain boundaries between different states, maintaining high neighbor-state correlation (positive ΔMI) with minimal movement. Near-zero Moran's I confirms these are local structures, not large-scale uniform clusters.

This taxonomy is based on qualitative inspection; formal feature-based clustering is available in the code repository (scripts/phenotype_taxonomy.py), which uses the features ΔMI, same-state adjacency fraction, state entropy, and predictability (Hamming) with deterministic thresholds (ΔMI > 0.12, adjacency > 0.60, entropy < 0.30) to assign each rule to one of four archetypes.

Statistical Significance

Table 3 presents Mann-Whitney U test results for the primary metric (neighbor MI) across all pairwise comparisons. All comparisons are highly significant after Holm-Bonferroni correction.

Table 3: Pairwise statistical tests for ΔMI (Eq. 2). Cliff's δ measures effect size (= rank-biserial r); bootstrap 95% CIs for the median difference (10,000 resamples) are the primary effect-size statistic; p-values (Holm-Bonferroni corrected) are secondary. Note that Cliff's δ measures stochastic dominance (probability that a random draw from one group exceeds the other), whereas the bootstrap CI estimates the location shift of the median difference. Effect-size interpretation: $\delta = 0.355$ (P1 vs. P2) is moderate-to-large; $\delta = 0.124$ (Ctrl vs. P1) is small but statistically reliable with $n > 2000$; median differences for Ctrl vs. P1 are < 0.001 bits, indicating practical equivalence in coordination level despite statistical detectability.

Comparison	Direction	n_1	n_2	Cliff's δ	Median diff 95% CI	p-value
P1 vs. P2	P2 > P1	3570	3735	0.355	[0.078, 0.111]	$< 10^{-252}$
Ctrl vs. P1	P1 > Ctrl	2225	3570	0.124	[$< 0.001, < 0.001$]	$< 10^{-50}$
Ctrl vs. P2	P2 > Ctrl	2225	3735	0.423	[0.078, 0.111]	≈ 0

Survival Analysis

Survival rates differ significantly across conditions (Table 2). Phase 2 achieves the highest survival rate, followed by Phase 1 and Control. State-uniformity is the dominant termination mode for the control condition, suggesting that without neighbor state information, rules frequently drive all agents to the same state.

Discussion

Observation richness as a driver of emergence. Our central finding is that the content of observation—specifically, access to neighbor state information—is the primary driver of emergent spatial coordination. This holds even when controlling for rule table size (the control condition). With shuffle-null-calibrated MI, Phase 2 is the only rule-based condition achieving nonzero median ΔMI, while both Phase 1 and Control fall to zero—making the qualitative separation between observation conditions unambiguous. The same-state adjacency fraction (Table 2) provides a categorical spatial statistic appropriate for nominal state data. Phase 2's adjacency fraction (0.350) exceeds the random-placement expectation (≈ 0.25 for 4 equiprobable states), confirming local coordination. Moran's I (reported in the supplementary material) is a secondary indicator, as it treats categorical states as numeric; nonetheless, it reveals that the Control condition exhibits the strongest spatial clustering (median $I = 0.124$) despite zero ΔMI, while Phase 2's near-zero median I (-0.020) indicates that its coordination operates at the local neighbor level rather than through large-scale spatial clustering. This result is not a consequence of having more rules to choose from, but of each rule being able to respond to richer local information.

Exploratory temporal pattern (not a primary claim). The temporal trajectories suggest a possible frozen–dynamic–chaotic ordering (Phase 1, Phase 2, Control), but we treat this strictly as exploratory context, not as evidence for edge-of-chaos theory. Establishing such a claim would require dedicated criticality analyses beyond the scope of the present work.

Viability filtering as minimal selection. Our methodology embodies a minimal philosophy: generate random configurations, remove only the degenerate ones (halt or state-uniformity), and examine what structure the survivors exhibit. We acknowledge that this "negative selection" constitutes a minimal selection pressure—surviving rules must avoid degenerate dynamics (halt or state uniformity)—but it is purely physical, imposing no behavioral or performance criterion. The surprising finding is that meaningful structure—quantified by mutual information—emerges even under this minimal regime, provided the observation channel is sufficiently rich.

Filter-metric independence. A potential concern is that viability filters might inadvertently select for high-MI rules, confounding the comparison between observation conditions. Point-biserial correlation between survival status and final-step MI yields $r = 0.14$ for Phase 2 ($p < 10^{-22}$), $r = 0.14$ for Phase 1, and $r = 0.45$ for Control. The Control's elevated correlation reflects its low survival rate (44.5% vs. $\sim$72% for rule-based conditions): stronger selection on survivors inflates the correlation mechanically. The relevant comparison is P1 and P2's near-identical $r \approx 0.14$, which indicates that the MI advantage of Phase 2 over Phase 1 is not an artifact of differential filter selection: both conditions have nearly identical filter-MI correlation, yet Phase 2 achieves substantially higher ΔMI.

Directional information flow. Transfer entropy analysis (supplementary material) confirms that the spatial coordination in Phase 2 involves genuine directional information flow from neighbor states to agent next-states, beyond what symmetric MI captures. This rules

out the possibility that the observed MI arises from static correlations without dynamic coupling.

Capacity-matched controls. To further isolate the role of observation content from table capacity, we evaluated two additional control conditions (supplementary material): (i) a capacity-matched Phase 1 with 100-entry tables aliased to 20 effective observations, and (ii) a random-encoding Phase 2 with randomly permuted neighborhood-to-observation mappings. Both controls produce ΔMI significantly below standard Phase 2, confirming that structured encoding of neighbor state information—not table size or alphabet size—drives coordination.

Spatial scrambling confirmation. Spatial scrambling analysis (supplementary material) confirms that Phase 2's elevated MI depends on genuine local spatial coordination: randomly reassigning agent positions while preserving states reduces MI to near-zero levels, consistent with the shuffle-null calibration.

Role differentiation and temporal signatures. Beyond MI, our metric suite reveals additional dimensions of emergent structure (supplementary material, Section L). The variance of per-agent action entropy captures whether agents specialize into distinct behavioral roles: high variance indicates emergent role differentiation, where some agents consistently select the same action while others explore. Phase 2's access to dominant neighbor state is expected to support greater differentiation than Phase 1 or Control, where agents cannot distinguish neighbor identity. Quasi-periodicity peaks and phase-transition $\max\Delta$ provide temporal signatures that complement the MI time-series analysis: recurrent oscillatory patterns and abrupt reorganization events, respectively. Cross-condition differences in these temporal metrics further support the observation-richness narrative.

Filter cascade robustness. The main experiments apply only weak viability filters (halt detection, state uniformity). A cascaded filter analysis (supplementary material, Section M) applies additional medium-strength filters—short-period detection and low-activity detection—to test whether the Phase 2 MI advantage persists under stricter viability criteria. If the observation-richness ordering (Control < P1 < P2) holds among the more stringently filtered survivors, it strengthens the claim that coordination is a genuine property of the rule–observation interaction, not an artifact of lax filtering.

Implications for ALife research. These results suggest that objective-free search deserves more attention as a complement to fitness-driven approaches. When the goal is to discover what is possible rather than to optimize for a specific outcome, removing the objective function may reveal phenomena that fitness landscapes obscure. The key enabler is not the search algorithm but the architecture of the agents—specifically, what they can observe.

Limitations

Several limitations constrain the generalizability of our findings:

- Single topology: All experiments use a 20×20 toroidal grid with von Neumann neighborhoods. Other topologies (hexagonal grids, Moore neighborhoods, irregular graphs) may produce different results.

- Symmetric metric: Mutual information is symmetric and measures correlation, not causation. Transfer entropy (supplementary material) confirms directional information flow in Phase 2, but a full time-resolved analysis remains for future work.

- No multi-generation evolution: Each rule table is evaluated in a single 200-step simulation. We do not evolve rules across generations, which limits comparison with evolutionary ALife systems.

- Small state space: With only 4 internal states and 9 actions, the model is deliberately minimal. Scaling to larger state spaces may reveal qualitatively different dynamics.

- Density fixed: The main experiments use 30 agents on a 400-cell grid (7.5% density). The supplementary material reports a systematic density sweep across 12 conditions (density range 0.017–0.400), confirming that the Phase 2 MI advantage holds across all tested densities.

- Sequential update order: Agents are updated in a random permutation each step, creating implicit temporal correlations between early and late updates within the same step. Synchronous update schemes may produce different dynamics.

- Single simulation per rule (main experiment): Each rule table is evaluated with a single initial configuration in the main experiment. The supplementary material provides multi-seed robustness analysis for the top 50 rules from each rule-based condition (Phase 2, Phase 1, and Control), confirming that MI levels—whether high, low, or zero—are stable properties of

the rule table, not seed-specific accidents. As a brief in-text summary: among the top 50 Phase 2 rules re-evaluated across 20 independent seeds, 84% maintain positive median ΔMI (mean $P(\Delta\text{MI} > 0) = 0.748$), compared to 36% for Phase 1 and 44% for Control.

- Halt window sensitivity: The main experiments use a 10-step halt window. A sensitivity sweep across $\{5, 10, 20\}$ (supplementary material) confirms that results are robust to this parameter choice: survival rates and MI distributions remain qualitatively unchanged.

- Ranking overlap boundary case: Kendall-τ ranking stability requires overlapping rule identities across batches. When overlap is zero, τ is not estimable and is reported as N/A. Overlap fraction is therefore a prerequisite diagnostic for interpreting ranking stability.

Conclusion

We have shown that meaningful spatial coordination emerges in a multi-agent system through objective-free but viability-filtered negative selection, and that the richness of agents' observation channels—not rule table capacity—is the critical factor. The evidence ladder from step-clock control through density-only to state-profile observation demonstrates a monotonic relationship between observation content and emergent coordination, confirmed by a bias-corrected MI estimator across all tested density levels (see the supplementary material).

Transfer entropy analysis (supplementary material) confirms directional information flow in Phase 2, and capacity-matched controls rule out table size as a confound. Future work should extend to larger grids and state spaces, explore multi-generation rule evolution under the same objective-free regime, and investigate whether richer observation channels enable qualitatively different forms of coordination. The broader implication is that the "remove broken, observe survivors" philosophy can serve as a productive complement to fitness-driven search in artificial life.

Supplementary Material. Density sweep analysis, multi-seed robustness results (all three rule-based conditions), halt-window sensitivity, survival rate confidence intervals, alternative null models, spatial scrambling analysis, transfer entropy, capacity-matched controls, algorithmic pseudocode, cross-condition metric profiles, and cascaded filter analysis are available as supplementary material with the code repository.

References

Bedau, M. A. (2003). Artificial life: Organization, adaptation and complexity from the bottom up. Trends in Cognitive Sciences, 7(11):505–512.

Chan, B. W.-C. (2019). Lenia: Biology of artificial life. Complex Systems, 28(3):251–286.

Cliff, N. (1993). Dominance statistics: Ordinal analyses to answer ordinal questions. Psychological Bulletin, 114(3):494–509.

Cover, T. M. and Thomas, J. A. (1991). Elements of Information Theory. Wiley.

Efron, B. (1979). Bootstrap methods: Another look at the jackknife. The Annals of Statistics, 7(1):1–26.

Gardner, M. (1970). Mathematical games: The fantastic combinations of John Conway's new solitaire game "life". Scientific American, 223(4):120–123.

Holm, S. (1979). A simple sequentially rejective multiple test procedure. Scandinavian Journal of Statistics, 6(2):65–70.

Lehman, J. and Stanley, K. O. (2008). Exploiting open-endedness to solve problems through the search for novelty. In Proceedings of the Eleventh International Conference on Artificial Life (ALIFE XI), pages 329–336.

Lehman, J. and Stanley, K. O. (2011). Abandoning objectives: Evolution through the search for novelty alone. Evolutionary Computation, 19(2):189–223.

Lizier, J. T., Prokopenko, M., and Zomaya, A. Y. (2012). Local measures of information storage in complex distributed computation. Information Sciences, 208:39–54.

Mann, H. B. and Whitney, D. R. (1947). On a test of whether one of two random variables is stochastically larger than the other. The Annals of Mathematical Statistics, 18(1):50–60.

Miller, G. A. (1955). Note on the bias of information estimates. In Quastler, H., editor, Information Theory in Psychology: Problems and Methods, pages 95–100. Free Press, Glencoe, IL.

Moran, P. A. P. (1950). Notes on continuous stochastic phenomena. Biometrika, 37(1/2):17–23.

Ofria, C. and Wilke, C. O. (2004). Avida: A software platform for research in computational evolutionary biology. Artificial Life, 10(2):191–229.

Ray, T. S. (1991). An approach to the synthesis of life. In Langton, C. G., Taylor, C., Farmer, J. D., and Rasmussen, S., editors, Artificial Life II, pages 371–408. Addison-Wesley.

Reynolds, C. W. (1987). Flocks, herds and schools: A distributed behavioral model. In Proceedings of the 14th Annual Conference on Computer Graphics and Interactive Techniques (SIGGRAPH '87), pages 25–34. ACM.

Stanley, K. O., Lehman, J., and Soros, L. (2019). Why open-endedness matters. Artificial Life, 25(2):33–42.

Taylor, T., Bedau, M., Channon, A., Ackley, D., Banzhaf, W., Beslon, G., Dolson, E., Froese, T., Hickinbotham, S., Ikegami, T., McMullin, B., Packard, N., Rasmussen, S., Virgo, N., Agmon, E., Clark, E., McGregor, S., Ofria, C., Ropella, G., Spector, L., Stanley, K. O., Stanton, A., Timperley, C., Vostinar, A., and Wiser, M. (2016). Open-ended evolution: Perspectives from the OEE workshop in York. Artificial Life, 22(3):408–423.

Wolfram, S. (1984). Cellular automata as models of complexity. Nature, 311(5985):419–424.